Biomass Accumulation and Clogging in Trickle-Bed Bioreactors

Ion Iliuta and Faïçal Larachi
Chemical Engineering Dept., Laval University, Québec, G1K 7P4, Canada

DOI 10.1002/aic.10201
Published online in Wiley InterScience (www.interscience.wiley.com).

Excessive biomass formation in two-phase flow trickle-bed bioreactors induces clogging and leads to the progressive obstruction of the bed that is accompanied with a buildup in pressure drop and flow channeling. Currently, physical models linking the two-phase flow to the space-time evolution of biological clogging are virtually nonexistent. An attempt has been made with this contribution to fill in this gap by developing a unidirectional dynamic multiphase flow model based on the volume-average mass, momentum, and species balance equations. Phenol biodegradation by Pseudomonas putida *as the predominant species immobilized on activated carbon was chosen as a case study to illustrate the consequences of formation of excessive amounts of biomass. Furthermore, in developing the transient model, the following basic processes were assumed to occur and have been accounted for in the mathematical model: oxygen transport from gas into liquid bulks, phenol, and oxygen transport from the liquid phase to the biofilm surface, simultaneous diffusion and reaction of phenol and oxygen within biofilm, as well as their simultaneous diffusion and adsorption within the porous supporting particles.* © 2004 American Institute of Chemical Engineers *AIChE J,* 50: 2541–2551, 2004
Keywords: trickle-bed reactors, biofilm, clogging, mathematical modeling.

Introduction

Classical trickle-bed bioreactors with biocatalysts immobilized on, or inside, the porous solid supporting particles have become increasingly important in carrying out, in through-flow manner, many types of waste-gas and wastewater treatment processes (Ottengraf et al., 1984, 1986; Leson and Winer, 1991). In trickle-bed bioreactors, biodegradable pollutants present in waste-gas or wastewater passing through the packed bed are transferred into the attached microbial film where microbiological degradation occurs, and are ultimately consumed. Since pollutant degradation occurs at normal temperature and pressure, biodegradation represents a potentially energy-efficient technology when compared to traditional physical and chemical abatement processes (for example, catalytic oxidation, incineration, absorption, or regenerative adsorption).

The pollutant removal efficiency in trickle-bed bioreactors is very sensitive to changes in the hydrodynamic conditions prevailing in the reactor. Two-phase flow in trickle-bed bioreactors is influenced by a large number of variables including the fluids physical characteristics (density and viscosity), the process variables (flow rates, temperature), the solid particles characteristics (size, shape, roughness, tortuosity, microporosity, effective diffusivity), the bed packing protocol, particle-to-column diameter ratio, and distributor design, and other features inherent to the biological and physical clogging. Therefore, improving the understanding of the two-phase flow coupled with the physical and microbiological phenomena taking place in trickle-bed bioreactors is vital for the accomplishment of successful and sustainable bioroute technology.

A major drawback limiting the use of trickle-bed bioreactors for biological waste-gas and wastewater treatments is ascribed to the clogging phenomenon induced by the formation of an excessive amount of biomass, which narrows the free interstitial space left to the fluids flow (van Lith et al., 1994; Weber and Hartmans, 1994; Sorial et al., 1995; Weber and Hartmans, 1996; Alonso et al., 1997; Cox and Deshusses, 1999, Okkerse et al., 1999). Excessive biomass formation and buildup leads to the progressive obstruction of the bed, and is accompanied with a rise in pressure drop and flow channeling. In these circumstances, for maintaining acceptable operating cycles, the unit

Correspondence concerning this article should be addressed to I. Iliuta at ion.iliuta@gch.ulaval.ca.

must be backwashed or shutdown regularly for removing the excess biomass.

Periodic interruption of the biological process for the excess biomass removal is the typical practical response (Schroeder, 2002). Periods of interruption may vary from a few minutes to several days. Little impact on performance is observed when the flow is stopped for periods of up to 12 h (Schroeder, 2002). When such interruptions become frequent or longer, the process operating costs may seriously become a major obstacle. Processes for excess biomass removal are mainly derived from three major types: physical/mechanical, chemical, and biological. Physical treatments consist mainly of bed stirring or in draining the accumulated biomass via water backwashing (Wübker et al., 1997; Laurenzis et al., 1998, Delhoménie et al., 2003). Chemical treatments use reagents that dissociate the chemical bonds between the biofilm and the supporting solid surfaces, or that directly degrade the biomass to a removable condition (Diks et al., 1994; Schonduve et al., 1996; Chen and Stewart, 2000; Delhoménie at al., 2003). Biological treatments utilize microorganisms that are able to degrade the biomass accumulated through the bed (Cox and Deshusses, 1997).

Several investigators in the past have attempted to describe the transient behavior of biomass accumulation in the case of trickle-bed bioreactors for *waste-gas treatment* (Deshusses et al., 1995; Alonso et al., 1997; Okkerse et al., 1999). Deshusses et al. (1995) developed a dynamic model that calculates the variation of the contaminant concentration over time assuming constant biofilm thickness and includes multiple-substrate degradation. Alonso et al. (1997) developed a dynamic model for biotreatment of a waste gas that includes biomass growth, and a variable biofilm thickness along the column. The authors also account for a decreasing mass-transfer coefficient in their system due to excessive biofilm formation upon the packing. Deactivation of biomass was neglected, as the assumption was made all biomass in the column is viable. Okkerse et al. (1999) developed a dynamic model that describes the degradation of volatile acidifying pollutants in biotrickling filters for waste gas purification, as well as the resulting mass accumulation in the system and mass distribution along the column. The model takes into account the reaction inhibition by the production of acid, and a distinction is made between active and inactive biomass.

In contrast, the literature still remains short about the complex hydrodynamics, physical, and microbiological phenomena involved in the clogging of trickle-bed bioreactors for *aerobic wastewater treatment* despite the critical operational problem of excessive biomass formation. There is a lack of descriptive and quantitative *reactor-scale* models, which can be used for predicting the fate of trickle-bed hydrodynamics under clogging conditions, and for planning strategies for minimizing the problem of clogging. It is, therefore, vital to gain new fundamental knowledge by tackling the complex hydrodynamics, physical, and microbiological phenomena involved in the clogging of trickle beds due to the formation of excessive amounts of biomass. This contribution is offered as a step in that direction and is a continuation of our endeavor (Iliuta et al., 2003; Iliuta and Larachi, 2003) in developing mathematical models for the description of two-phase flow and space-time evolution of clogging in gas-liquid-solid reactors.

In this work, a one-dimensional (1-D) two-fluid model based on the volume-average mass, momentum, and species balance

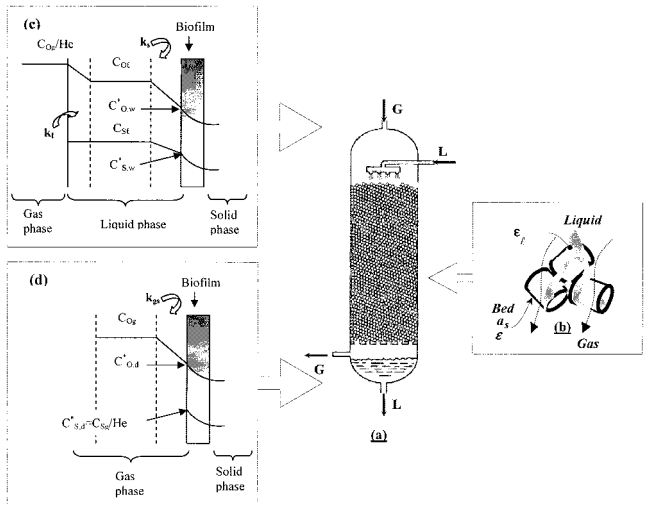

Figure 1. (a) Trickle-bed bioreactor; and (b) local scale representation of the two-phase flow; (c) resistances involved in the G/L reaction on the biofilm when the external surface area of the biocatalyst particle is completely wetted; and (d) the external surface area of the biocatalyst particle is completely dry.

equations is developed for the description of the two-phase flow and space-time evolution of biological clogging in trickle-bed bioreactors for wastewater treatment. Phenol biodegradation by *Pseudomonas putida* as the predominant species immobilized on activated carbon was chosen as a case study illustrating the consequences of formation of excessive amount of biomass. Also, in developing the mathematical model the following basic processes were assumed: transport of oxygen from the gas phase into liquid phase, transport of phenol and oxygen from the liquid phase to the surface of the biofilm, simultaneous diffusion, and reaction of phenol and oxygen within the biofilm, and simultaneous diffusion and adsorption of phenol, and diffusion of oxygen in the activated carbon particles. The impact of the formation of an excessive amount of biomass is evaluated in terms of pressure drop rise as a function of time, as well as in terms of clogging patterns, for example, local porosity, and biofilm thickness versus bed depth. In our previous works (Iliuta et al., 2003; Iliuta and Larachi, 2003) only the feed liquid was considered as a source for clogging without considering the solids generated in the packed bed. In this work, our objective is to study clogging due to biosolid deposition resulting from a biochemical reaction.

Mathematical Model Development

A cocurrent downward gas-liquid *trickle flow* through a porous medium of uniform initial porosity ε^o and single-sized particles is considered (Figure 1a). Two-phase flow was assumed unidirectional and both the flowing phases are assumed as viscous Newtonian. The liquid was incompressible and the gas phase was ideal. The gas/liquid/biofilm/porous medium multiphase system is viewed as a system of three interpenetrated continua: (1) a flowing gas phase; (2) a flowing liquid phase; (3) and a stationary *pseudocontinuous* solid phase made up of the packing particles constituting the clean porous me-

dium, as well as of the biomass captured onto their surface. The phenol biodegradation by *Pseudomonas putida* as the predominant species immobilized on activated carbon was considered.

Further assumptions inherent to the formulation developed in this work are:

- The bed is partially wetted by the liquid phase (Figure 1b).
- Two-phase flow is annular and completely separated.
- Each phase, that is, gas, liquid, and solid, behaves as a continuum so that the macroscopic differential balance equations can be applied, however, except for the solid mass conservation, the solid stress balance is not included in this analysis.
- The coupling between the fluid and solid phases is monitored via the interfacial drag forces (Eqs.29–31).
- The organics are nonvolatile and the reaction is taking place solely on the biofilm contacted by liquid.
- The consumption of both phenol and oxygen by the suspended bioflocs sloughed off from the bioparticles is negligible as compared to the consumption by bioparticle.
- The concentration level of pollutant in the feedstream is low so that the reactor is isothermal (25° C).
- For the analysis of the external gas-liquid and liquid-solid mass-transfer processes, the film model is used.
- At the gas-liquid interface, the Henry law relating O_2 partial pressure to oxygen solubility is valid.

The model was based on the volume average form of the transport equations for multiphase systems (Whitaker, 1973). The model equations consist of the conservation of volume, conservation of mass or continuity, conservation of momentum for the gas and liquid phases, continuity for the solid *stationary* phase (that is, the fixed bed), and species balance in the gas and liquid phases:

Conservation of volume

$$\varepsilon_\ell + \varepsilon_g = \varepsilon \tag{1}$$

Continuity for the gas and liquid phases

$$\frac{\partial}{\partial t}\,\varepsilon_g\rho_g + \frac{\partial}{\partial z}\,\varepsilon_g\rho_g u_g = 0 \tag{2}$$

$$\frac{\partial}{\partial t}\,\varepsilon_\ell\rho_\ell + \frac{\partial}{\partial z}\,\varepsilon_\ell\rho_\ell u_\ell = 0 \tag{3}$$

Continuity for the solid phase

$$\frac{\partial}{\partial t}[(1-\varepsilon^o)\rho_s + (\varepsilon^o-\varepsilon)\rho_v] = D^{\text{eff}}_{S,b}\left.\frac{dC_{S,w}}{dr}\right|_{r=r_b} a_{sb}(1-\varepsilon)\eta_e\frac{Y_{X/S}}{\rho_v} + D^{\text{eff}}_{S,b}\left.\frac{dC_{S,d}}{dr}\right|_{r=r_b} a_{sb}(1-\varepsilon)(1-\eta_e)\frac{Y_{X/S}}{\rho_v} \tag{4}$$

Momentum balance equations for the gas and liquid phases

$$\frac{\partial}{\partial t}\,(\rho_g\varepsilon_g u_g) + u_g\frac{\partial}{\partial z}\,(\rho_g\varepsilon_g u_g) = \varepsilon_g\mu^e_g\frac{\partial^2 u_g}{\partial z^2} - \varepsilon_g\frac{\partial P}{\partial z} + \varepsilon_g\rho_g g - F_{g\ell} - F_{gs} \tag{5}$$

$$\frac{\partial}{\partial t}\,(\rho_\ell\varepsilon_\ell u_\ell) + u_\ell\frac{\partial}{\partial z}\,(\rho_\ell\varepsilon_\ell u_\ell) = \varepsilon_\ell\mu^e_\ell\frac{\partial^2 u_\ell}{\partial z^2} - \varepsilon_\ell\frac{\partial P}{\partial z} + \varepsilon_\ell\rho_\ell g + \frac{\varepsilon\eta_e - \varepsilon_\ell}{\varepsilon_g}[F_{g\ell} + F_{gs}] - F_{\ell s} \tag{6}$$

Species balance in the liquid phase (axial dispersion in the liquid phase)

$$\frac{\partial}{\partial t}\,(C_{S\ell}\varepsilon_\ell) + u_\ell\frac{\partial}{\partial z}\,(C_{S\ell}\varepsilon_\ell) = D_\ell\frac{\partial^2}{\partial z^2}\,(C_{S\ell}\varepsilon_\ell) - D^{\text{eff}}_{S,b}\left.\frac{dC_{S,w}}{dr}\right|_{r=r_b} a_{sb}(1-\varepsilon)\eta_e \tag{7}$$

$$\frac{\partial}{\partial t}\,(C_{O,\ell}\varepsilon_\ell) + u_\ell\frac{\partial}{\partial z}\,(C_{O,\ell}\varepsilon_\ell) = D_\ell\frac{\partial^2}{\partial z^2}\,(C_{O,\ell}\varepsilon_\ell) + k_\ell a(C_{Og}/He - C_{O\ell}) - D^{\text{eff}}_{O,b}\left.\frac{dC_{O,w}}{dr}\right|_{r=r_b} a_{sb}(1-\varepsilon)\eta_e \tag{8}$$

Species balance in the gas phase (no axial dispersion in the gas phase)

$$\frac{\partial}{\partial t}\,(C_{O,g}\varepsilon_g) + u_g\frac{\partial}{\partial z}\,(C_{O,g}\varepsilon_g) = -k_\ell a(C_{Og}/He - C_{O\ell}) - D^{\text{eff}}_{O,b}\left.\frac{dC_{O,d}}{dr}\right|_{r=r_b} a_{sb}(1-\varepsilon)(1-\eta_e) \tag{9}$$

Here, P stands for pressure, ε_α, ρ_α, and u_α represent, respectively, the holdup, the density, and the longitudinal (interstitial) velocity of phase α (gas or fluid phases), while the subscripts s and b refer to the solid phase and biofilm, respectively. $F_{\alpha\beta}$ represents the interfacial drag force per unit reactor volume exerted at the interface between mutually interacting α and β phases (gas, fluid, and solid phases). The α-phase effective viscosity μ^e_α, which arises from the combination of the viscous and the pseudoturbulence stress tensors is formulated as proposed by Dankworth et al. (1990). In addition, g is the acceleration due to gravity, ε is the local porosity at time t, ε^o is the initial "clean" bed porosity, C_j is the concentration of j component, ρ_v is the total dry biomass in the biofilm, and η_e is the external wetting efficiency. Note that in the formulation of the momentum balance equations, the capillary pressure between phase λ and phase g is neglected.

Velocities at the inlet are specified in Dirichlet-type boundary conditions. At the outlet, an open boundary condition referred to as "outflow boundary condition" (Gresho and Sani, 1998) was used. Outflow boundary conditions are usually appropriate to model exit flows where velocity and pressure distributions are not known *a priori*. They are appropriate when exit flows are fully developed or close to, which implies, except for pressure, zero gradients for all flow variables normal to the outflow boundary. The liquid hold-up at the reactor inlet was calculated assuming $du_g/dz = du_\ell/dt = 0$ and combining Eqs. 5 and 6

$$\frac{F_{g\ell}}{\varepsilon_g}\left[1+\frac{\varepsilon\eta_e-\varepsilon_\ell}{\varepsilon_\ell}\right]+\frac{F_{gs}}{\varepsilon_g}\left[1+\frac{\varepsilon\eta_e-\varepsilon_\ell}{\varepsilon_\ell}\right]-\frac{F_{\ell s}}{\varepsilon_\ell}+(\rho_\ell-\rho_g)\,g=0 \quad (10)$$

Initial and boundary conditions for Eqs. 7 – 9 are

$$t=0 \quad C_{j\ell}=C_{j\ell}^{\text{in}},\ C_{Og}=C_{Og}^{\text{in}} \quad \text{where} \quad j=PhOH,\ O_2 \quad (11)$$

$$z=0 \quad u_\ell C_{j\ell}^{\text{in}}=u_\ell C_{j\ell}\big|_{z=0^+}-D_\ell\frac{\partial C_{j\ell}}{\partial z} \quad \text{where} \quad j=PhOH,\ O_2 \quad (12)$$

$$C_{Og}=C_{Og}^{\text{in}} \quad (13)$$

$$z=H \quad \frac{\partial C_{j\ell}}{\partial z}=0 \quad \text{where} \quad j=PhOH,\ O_2 \quad (14)$$

The solution of Eqs. 4, 7–9 requires knowledge of the concentration profiles of phenol and oxygen within the bioparticle (Figures 1c and 1d). These concentration profiles are governed by the diffusional flux of phenol and oxygen within the bioparticle, the kinetics of consumption of both phenol and oxygen by cells constituting the biofilm, and the adsorption/desorption of phenol by the activated carbon particle. Formulation of equations describing the simultaneous transport, reaction, and adsorption/desorption of phenol and oxygen within the bioparticles is based on the following assumptions:

- Both the activated carbon particles and the bioparticles are spherical in shape and uniform in size.
- The microorganisms are uniformly distributed over the surface of activated carbon particles forming a uniform biofilm.
- The biofilm is assumed to be a homogeneous matrix within which phenol and oxygen diffuse according to Fick's law, and are consumed by microorganisms.
- The various species of microbes present in the biofilm can be treated as a single *lumped* species. Accordingly, the biological parameters used to depict the activity of a pure culture can be employed to describe the metabolic activity of such a lumped species.
- The growth-limiting nutrients are phenol and oxygen; all other nutrients are present in excess.
- There is no physiological change of the microbes when immobilized onto the activated carbon particles, so that the kinetic expression of cell growth and substrate degradation obtained from a suspended cell culture can be applied equally well to the immobilized system.
- Effects of outward diffusion of metabolic products are negligible.
- Due to the inhibitory nature of phenol to the microorganisms (Tang et al., 1987), the Haldane equation was used to describe the growth kinetics of the culture:

$$\mu=\frac{\mu_{\max}C_S}{K_s+C_S+C_S^2/K_i}\frac{C_O}{K_{ox}+C_O} \quad (15)$$

- The effects of depletion of both phenol and oxygen due to adsorption in the biofilm are negligible, and adsorption of oxygen by activated carbon is negligible.
- The internal wetting of the solid spherical particles was considered complete, and the reactants' diffusion inside the particle occurs in the liquid phase.

According to the above assumptions, the simultaneous transport and consumption of phenol and oxygen within the biofilm (the external surface area of the catalyst particle is completely wetted or completely dry) can be given by

$$\varepsilon_b\frac{\partial C_S}{\partial t}=\frac{1}{r^2}\frac{\partial}{\partial r}\left(r^2D_{S,b}^{\text{eff}}\frac{\partial C_S}{\partial r}\right)-\frac{\mu\rho_v}{Y_{X/S}} \quad (16)$$

$$\varepsilon_b\frac{\partial C_O}{\partial t}=\frac{1}{r^2}\frac{\partial}{\partial r}\left(r^2D_{O,b}^{\text{eff}}\frac{\partial C_O}{\partial r}\right)-\frac{\mu\rho_v}{Y_{X/O}} \quad (17)$$

in which ε_b is estimated from $(1-\rho_v/\rho_c)$ (Tang et al., 1987).

The simultaneous diffusion of both phenol and oxygen and adsorption within the activated carbon particles are given by

$$\varepsilon_p\frac{\partial C_S}{\partial t}+\rho_s\frac{\partial q}{\partial t}=\frac{1}{r^2}\frac{\partial}{\partial r}\left(r^2D_{S,p}^{\text{eff}}\frac{\partial C_S}{\partial r}\right) \quad (18)$$

$$\varepsilon_p\frac{\partial C_O}{\partial t}=\frac{1}{r^2}\frac{\partial}{\partial r}\left(r^2D_{O,p}^{\text{eff}}\frac{\partial C_O}{\partial r}\right) \quad (19)$$

Equation 18 may be rearranged to give

$$\frac{\partial C_S}{\partial t}=\frac{D_{S,p}^{\text{eff}}}{\varepsilon_p+\rho_s\dfrac{dq}{dC_S}}\frac{1}{r^2}\frac{\partial}{\partial r}\left(r^2\frac{\partial C_S}{\partial r}\right) \quad (20)$$

where dq/dC_S is the first derivative of the adsorption isotherm of phenol by activated carbon particles.

The activated carbon particles with the biofilm completely removed were found to be reversible in the adsorption/desorption of phenol (Tang et al., 1987). The Langmuir equation was used to describe the adsorption/desorption isotherm in the following expression

$$q=\frac{3825.3C_S}{1+25.329C_S} \quad (21)$$

The corresponding boundary and initial conditions for Eqs. 16, 17, 19, and 20 are given as

$$r=0 \quad \frac{\partial C_S}{\partial r}=\frac{\partial C_O}{\partial r}=0 \quad (22)$$

$$r=r_p \quad D_{S,b}^{\text{eff}}\frac{\partial C_S}{\partial r}\bigg|_{r=r_p^+}=D_{S,p}^{\text{eff}}\frac{\partial C_S}{\partial r}\bigg|_{r=r_p^-} \qquad D_{O,b}^{\text{eff}}\frac{\partial C_O}{\partial r}\bigg|_{r=r_p^+}=D_{O,p}^{\text{eff}}\frac{\partial C_O}{\partial r}\bigg|_{r=r_p^-} \quad (23)$$

$$C_S|_{r_p^-} = C_S|_{r_p^+} \quad C_O|_{r_p^-} = C_O|_{r_p^+} \tag{24}$$

$r = r_b$ the external surface area of the catalyst particle is completely wetted (to calculate η_ℓ)

$$D_{S,b}^{\text{eff}} \frac{\partial C_S, w}{\partial r}\bigg|_{r=r_b} = k_{s,S}(C_{S,\ell} - C_{S,w}^*)$$

$$D_{O,b}^{\text{eff}} \frac{\partial C_{O,w}}{\partial r}\bigg|_{r=r_b} = k_{s,O}(C_{O,\ell} - C_{O,w}^*) \tag{25}$$

the external surface area of the catalyst particle is completely dry (to calculate η_g)

$$C_{S,d}^* = C_{Sg}/He \quad D_{O,b}^{\text{eff}} \frac{\partial C_{O,d}}{\partial r}\bigg|_{r=r_b} = k_{gs,O}(C_{O,g} - C_{O,d}^* He) \tag{26}$$

$$t = 0 \quad C_S(r, 0) = C_{S,\ell}^{\text{in}} \quad C_O(r, 0) = C_{O,\ell}^{\text{in}} \tag{27}$$

Because the biofilm thickness increases with time during the transient state, the system of Eqs. 16, 17 is a moving boundary problem. Since the microorganisms are uniformly distributed over the surface of activated carbon particles forming a uniform biofilm, the biofilm thickness was estimated at any time by means of the following relationship

$$\delta_b = \frac{\varepsilon^o - \varepsilon}{a_s^o} \tag{28}$$

To make the system solvable, the conservation equations Eqs.1–9, 16, 17, 19, 20 for the 13 unknowns, that is, ε_ℓ, ε_g, ε, u_ℓ, u_g, P, $C_{j,\ell}$ and C_j must be augmented by auxiliary closure relations for the gas-liquid ($F_{g\ell}$), gas-solid (F_{gs}), and the liquid-solid ($F_{\ell s}$) interfacial drag forces.

Interfacial drag forces. The assumption of bed partial wetting entrains that the gas-phase drag will have contributions due to effects located at the gas-liquid ($F_{g\ell}$) and gas-solid (F_{gs}) interfaces. Similarly, the resultant of the forces exerted on the liquid phase involves two components: (1) the drag force, $F_{\ell s}$, experienced by the liquid due to the shear stress nearby the liquid-solid boundary, and (2) the gas-liquid interfacial drag due to the slip between fluids $F_{g\ell}$.

Under the circumstances of trickle flow, the double slit flow analogy yields a satisfactory approximation of the constitutive equations needed for the gas-liquid, liquid-solid and gas-solid drag forces (Iliuta et al., 2000). The double slit flow becomes well representative of the gas-continuous flow regimes when the liquid texture is mainly contributed by packing-supported liquid films and rivulets, and the gas-liquid separated flow and gas flow assumption holds. This generally occurs at low liquid flow rates that allow the transport of liquid in the form of a smooth and stable film (Holub et al., 1992). The actual trickle flow structure being conceptualized via a simplified cell of two parallel interconnected inclined slits (a gas-liquid slit corresponding to the region $a_s\eta_e$, and a dry slit corresponding to the region), the force balance equations for the gas and liquid are first solved in the slit scale and, thence, mapped into the bed scale. At a given depth z in the bed, the projections of the drag forces take the following forms (Iliuta et al., 2002)

$$F_{\ell s} = \eta_e \left\{ \frac{E_1}{36} C_w^2 \frac{a_{sb}^2(1-\varepsilon)^2 \mu_\ell \eta_e}{\varepsilon_\ell^3} + \frac{E_2}{6} C_{wi} \frac{a_{sb}(1-\varepsilon)}{\varepsilon_\ell^3} \rho_\ell \left| v_\ell \right| \right\} v_\ell \varepsilon_\ell \tag{29}$$

$$F_{gs} = (1-\eta_e) \left\{ \frac{E_1}{36} C_w^2 \frac{a_{sb}^2(1-\varepsilon)^2 \mu_g}{\varepsilon^3} + \frac{E_2}{6} C_{wi} \frac{a_{sb}(1-\varepsilon)}{\varepsilon^3} \rho_g \left| v_g \right| \right\} v_g \varepsilon \tag{30}$$

$$F_{g\ell} = \eta_e \left\{ \frac{E_1}{36} C_w^2 \frac{a_{sb}^2(1-\varepsilon)^2 \mu_g}{(\varepsilon - \varepsilon_\ell/\eta_e)^2 \varepsilon_g} + \frac{E_2}{6} C_{wi} \frac{a_{sb}(1-\varepsilon)\rho_g}{(\varepsilon - \varepsilon_\ell/\eta_e)^2 \varepsilon_g} \left| v_g - (\varepsilon - \varepsilon_\ell/\eta_e) u^* \right| \right\} [v_g - (\varepsilon - \varepsilon_\ell/\eta_e) u^*] \varepsilon_g \tag{31}$$

Here v_λ and v_g are the superficial velocities of the flowing phases, based on the total cross-sectional area of the reactor. E_1 and E_2 are the bed Ergun viscous and inertial constants. C_w and C_{wi} are the wall correction functions introduced here for, respectively the viscous and the inertial terms (Liu et al., 1994). Each one of the drag force expressions above involves a viscous contribution proportional to velocity, and an inertial term expressed in a quadratic velocity dependence. For an adaptation to the biofilm clogging context, these drag equations are recast as local functions of the local instantaneous values of the porosity, and of the effective specific surface area a_{sb} of the bioparticle. This latter is used instead of the particle diameter, because the effective specific surface area changes as microorganisms buildup onto the surface of the solid particles. The specific area of the bioparticle was estimated at any time with the following relationship

$$a_{sb} = \frac{6}{d_b} \tag{32}$$

where d_b is the diameter of the bioparticle:

$$d_b = d_p + 2\delta_b \tag{33}$$

To represent the gas-fluid relative motion intervening in $F_{g\lambda}$, the effect of slip between the gas and liquid is accounted for by means of the velocity u* at the gas-liquid interface derived in Iliuta et al. (2002) and estimated from the double slit model as

$$u^* = \frac{72}{E_1} \frac{\varepsilon_\ell}{(1-\varepsilon)^2 a_{sb}^2 \eta_e^2 \mu_\ell} \left[\frac{1}{2} \left(-\frac{\Delta P}{H} + \rho_\ell g \right) \varepsilon_\ell + \left(-\frac{\Delta P}{H} + \rho_g g \right) (\varepsilon \eta_e - \varepsilon_\ell) \right] \tag{34}$$

Method of solution. In order to solve the system of partial differential equations, we discretized in space and solved the

Table 1. Values of Kinetic Parameters

Kinetic Parameter	Value
μ_{max}, h^{-1}	0.365
K_s, mg/L	10.948
K_i, mg/L	113.004
K_{ox}, mg/L	0.1
$Y_{X/O}$, mg oxygen/mg phenol	0.354
$Y_{X/S}$, mg cell/mg phenol	0.496

resulting set of ordinary differential equations. The spatial discretization is performed using the standard cell-centered finite difference scheme (at the reactor level), and the method of orthogonal collocation (at the solid particle and biofilm level). The number of collocation points specified for the biofim and activated carbon particle was restricted to 5. The GEAR integration method for stiff differential equations was employed to integrate the time derivatives. Simulations are carried out on a Pentium® IV processor running at 2500 MHz. The relative error tolerance for the time integration process in the present simulations is set at 10^{-5} for each time step.

Results and Discussion

Model parameters' estimation.

To make the model solvable, the Ergun constants (E_1 and E_2), the volumetric gas-liquid ($k_\ell a$), liquid-solid (k_s) and gas-solid (k_{gs}) mass-transfer coefficients, the liquid axial-dispersion coefficient (D_ℓ), the external wetting efficiency (η_e), and the diffusivities of phenol and oxygen within the biofilm and kinetic parameters need to be specified. The Ergun single-phase flow parameters can be set either by measurements of single-phase pressure drops (Holub et al., 1992), or estimated from literature correlations (Iliuta et al., 1998). The volumetric gas-liquid mass-transfer coefficient and liquid-solid mass-transfer coefficient were estimated using recent literature correlations (Iliuta et al., 1999; Larachi et al., 2003). The gas-side mass-transfer coefficient across the dry pellet region was calculated from the correlation of Goto and Smith (1975). The wetting efficiency was evaluated using the comprehensive neural network correlation developed by Larachi et al. (2001a). The effective diffusion coefficient was evaluated assuming a tortuosity factor equal to 3. The extent of back-mixing in the liquid phase is quantified in terms of an axial dispersion coefficient which is evaluated using a recent comprehensive Bodenstein number correlation (Piché et al., 2002). For the gas phase, previous experimental and theoretical investigations indicated marginal importance of axial mixing so that plug flow is assumed for this phase. Diffusivities of phenol and oxygen within the biofilm were calculated using the correlation developed by Tang et al. (1987)

$$\frac{D_{j,\text{water}}}{D_{j,b}^{\text{eff}}} - 1 = 15.549\exp[-321.812(r_b - r_p)] \qquad (35)$$

where r_b and r_p are expressed in cm.

The kinetics parameters describing the growth of the microbial culture were determined by Tang and Fan (1987), see Table 1.

Model verification

There is no single work in the literature about two-phase flow and space-time evolution of biomass accumulation in trickle-bed bioreactors that could be used for validation of the proposed general approach. However, the simplified variant of our approach based on the steady-state volume-averaged species balance equations at the reactor level (Eqs. 7–9), coupled with the simultaneous transport and consumption of phenol and oxygen within the biofilm (Eqs. 16 and 17), and with the simultaneous diffusion of both phenol and oxygen and adsorption of phenol within the activated carbon particles (Eqs. 19 and 20), was compared to the experimental results obtained by Wisecarver and Fan (1989) and Hirata et al. (1986), in a gas-liquid-solid fluidized-bed bioreactor. In this simplified model, gas and liquid holdups were estimated using the recent literature correlations developed by Larachi et al. (2001b), and liquid axial dispersion coefficient was determined from the correlation of Kato et al. (1972). The correlations presented by, respectively, Shah et al. (1982) and Arters and Fan (1986) were used for the determination of gas-liquid and liquid-solid mass-transfer coefficients. Table 2 shows a comparison between the experimental results obtained by Wisecarver and Fan (1989) and Hirata et al. (1986) in a gas-liquid-solid fluidized-bed reactor with activated carbon particles (d_p=307 μm), respec-

Table 2. Comparison of Model Predictions with Experimental Results (Wisecarver and Fan, 1989; Hirata et al., 1986) ($c_{O,\ell}^{\text{in}}$ = 2 mg/l, $c_{O,g}^{\text{in}}$ = 275 mg/l)

v_ℓ, m/s	v_g, m/s	$C_{S,\ell}^{\text{in}}$, mg/L	δ_b, μm	ρ_v, mg/L	Phenol conversion (experimental)	Phenol conversion (predicted)
0.00015	0.0076	242	41.2	78000	0.9967*	0.9950
0.00015	0.0076	256	59.8	81000	0.9984*	0.9962
0.00015	0.0076	262	22.8	70000	0.9985*	0.9975
0.00015	0.0076	256	88.8	73000	0.9984*	0.9995
0.00015	0.0076	220	123.3	47000	0.9964*	0.9995
0.00015	0.0076	245	31.6	74000	0.9976*	0.9985
0.00015	0.0076	192	28.5	73000	0.9995*	0.9982
0.00015	0.0076	240	29.1	73000	0.9996*	0.9982
0.0022	0.0015	97.1	346	15000	0.4222&	0.4156
0.0026	0.0081	117.5	181	30000	0.6025&	0.5981
0.0045	0.0015	96.0	302	16000	0.2274&	0.2212
0.0050	0.0025	51.7	308	16000	0.5354&	0.5280

*Data from Wisecarver and Fan (1989)
&Data from Hirata et al. (1986)

Table 3. Parameters Used in Simulations

Temperature, °C	25
Pressure, atm	1.0
Reactor diameter, m	0.051
Bed height, m	0.9
Diameter of support particle, m	0.003
Density of support particle, kg/m^3	1400
Internal porosity	0.575
External porosity	0.37
Superficial liquid velocity, m/s	0.0015
Superficial gas velocity, m/s	0.0283
Dry cell mass/wet cell volume, mg/l (Chiam and Haris, 1983)	670000
Total dry biomass in the biofilm/wet biofilm volume, mg/L	15000–75 000
Henry's law constant	30

tively, with cement balls (d_p=388 and 623 μm) as the support particles, and the results predicted from the earlier model simplified by assuming hydrodynamic conditions as they prevail in a fluidized-bed bioreactor. It can be seen that there is an excellent agreement between the model predictions and experimental results. This agreement reflects the validity of the model over a wide range of biofilm thicknesses.

Simulations

Clogging is a complex phenomenon determined by such diverse factors as the biological and physical characteristics of the compounds involved, for example, microbial degradation rates and Henry constants, mechanical strength and morphology of the formed biofilm (especially its density), and structural characteristics of the packing material (Okkerse et al., 1999). Clogging in two-phase flow porous media in trickle-bed bioreactor systems is complex; flow field imaging of the transient phenomena accompanying fluid flow and biomass accumulation is not trivial, and has not been experimentally attempted yet. It is proposed here to test the model potentiality through simulations of different experimental configurations by solving the transport equations for the trickle-bed bioreactors. Clogging tests are run for phenol biodegradation by *Pseudomonas putida* as the predominant species immobilized on spherical activated carbon particles. The simulated conditions are listed in Table 3. To illustrate the quantitative and qualitative features of the clogging in trickle flow regime, the simulated results shown later are presented: (1) in terms of longitudinal profile snapshots of the local porosity and biofilm thickness; (2) as well as in the form of transient pressure drop buildup at different inlet phenol concentrations, total dry biomass in the biofilm, bed porosity, and particle diameter.

Because phenol biodegradation rate is more noticeable at low inlet phenol concentration (at inlet phenol concentrations higher than 50 mg/L, the cell growth rate decreases due to substrate inhibition, see Iliuta, 1997), the following simulations were undertaken for these conditions. To treat wastewater containing high-phenol concentration, either the residence time of wastewater in the reactor must be increased (by decreasing the wastewater influent flow rate or by increasing the reactor volume), or the wastewater must be diluted before feeding into the reactor (Tang and Fan, 1987).

Figures 2 and 3 show snapshots of the longitudinal profiles of the local porosity and the corresponding biofilm thickness for an inlet phenol concentration of 20 mg/L. In these figures

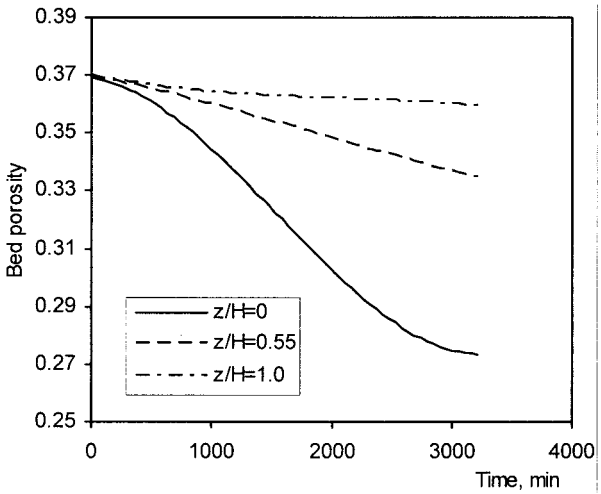

Figure 2. Variation of the bed porosity with the dimensionless axial distance, and the time ($C^{in}_{O,\ell}$ = 6 mg/l, $C^{in}_{O,g}$ = 275 mg/l, $C^{in}_{S,\ell}$ = 20 mg/l, ρ_v = 75 000 mg/l).

(and in the next ones), $t = 0$ represents the time corresponding to a biofilm thickness of 1micron. From these figures, it is clear that the biomass is not uniformly distributed along the column, and, as a consequence, the extent of clogging depends on axial distance. There is a noticeable decrease in local porosity in the entrance section of the bed that is coherent, and also mirrored by the increased biofilm thickness. As time evolves, the clogging front progressively fills up the column. However, biomass accumulation (clogging) is more confined in the entrance region, even if the overall effectiveness factor (the overall effectiveness factor was defined as a weighted sum of the effectiveness factors for completely dry particle and fully wetted particle: Ramachandran and Smith, 1979) is lower (Figure 4), because the cell growth rate is higher in this region. Toward the outside of the bioreactor, the cell growth rate decreases due to

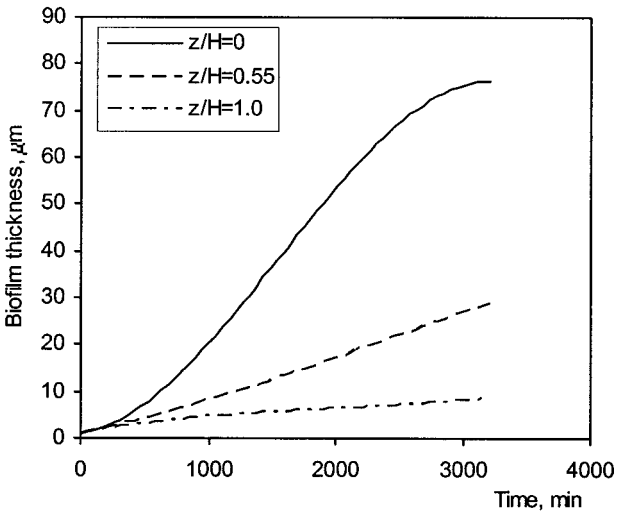

Figure 3. Variation of the biofilm thickness with the dimensionless axial distance, and the time ($C^{in}_{O,\ell}$ = 6 mg/l, $C^{in}_{O,g}$ = 275 mg/l, $C^{in}_{S,\ell}$ = 20 mg/l, ρ_v = 75 000 mg/l).

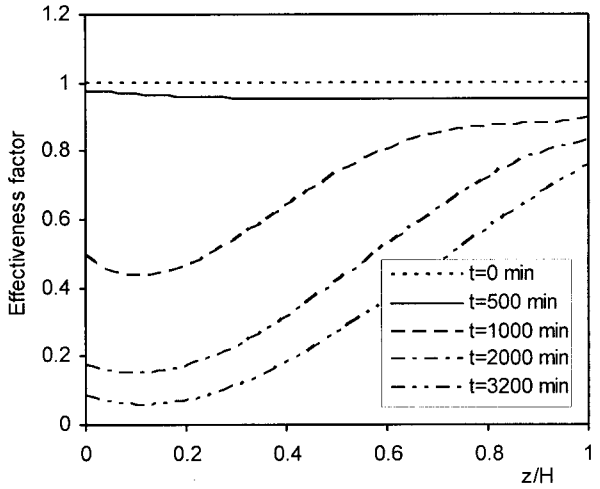

Figure 4. Variation of the effectiveness factor with the dimensionless axial distance and the time ($C^{in}_{O,\ell}$ = 6 mg/L, $C^{in}_{O,g}$ = 275 mg/L, $C^{in}_{S,\ell}$ = 20 mg/L, ρ_v = 75 000 mg/L).

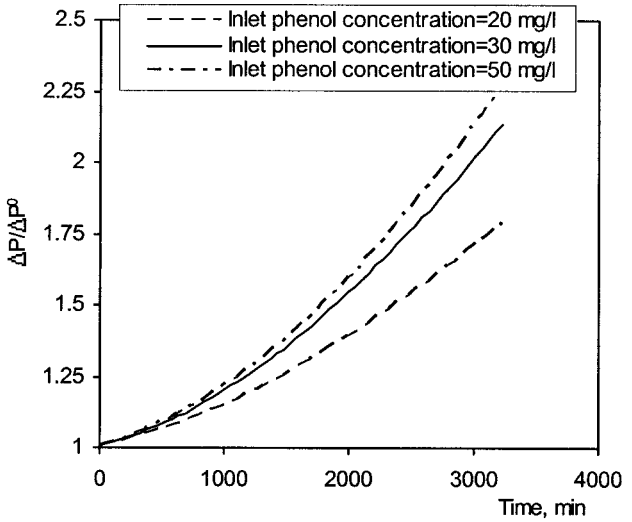

Figure 6. Two-phase pressure drop ratio versus time at different values of inlet phenol concentration ($C^{in}_{O,\ell}$ = 6 mg/L, $C^{in}_{O,g}$ = 275 mg/L, ρ_v = 75 000 mg/L).

the decrease in phenol concentration (Figure 5) and, as a result, the biomass accumulation is much lower that in the entrance section. As a consequence, the increase of the biofilm thickness and, respectively, the decrease of the local-bed porosity are much lower. The biofilm profiles (Figure 3) suggest that progression of biofilm accumulation exhibits sigmoid behavior. Such progression can practically be divided into three zones: (1) induction with biofilm thickness neighboring *ca.* 1 micron; (2) exponential or log accumulation; and (3) a plateau or steady-state zone (see curve at $z/H=0$, see Figure 3).

The relevant criterion for clogging is the pressure drop in the column. Figure 6 shows the effect of the inlet phenol concentration on the $\Delta P/\Delta P^o$ ratio (where ΔP^o is the two-phase pressure drop for the clean bed under otherwise identical conditions). With the increase of inlet phenol concentration, both the cell growth rate (Wisecarver and Fan, 1989; Iliuta, 1997) and the biomass accumulation increase, yielding higher biofilm thickness. As a result, the bed porosity decreases and the two-phase pressure drop increases. So, the major change resulting from biomass accumulation in the bed involves the effective porosity of the bed, and, therefore, the increase of two- phase pressure drop is the result of the decrease in the available free space. Consequently, the major change resulting from biomass accumulation in the bed involves the bed porosity, and, therefore, the pressure drop rise is mainly ascribed to a loss in available free space for gas flow.

A decrease in the value of total dry biomass in the biofilm (ρ_v) causes an increase in biofilm thickness (Figure 7), and a lower-bed porosity which translate into a higher buildup in

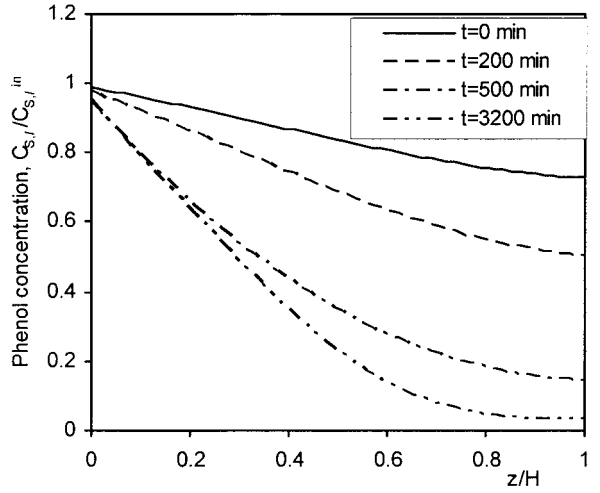

Figure 5. Variation of the phenol concentration with the dimensionless axial distance and the time ($C^{in}_{O,\ell}$ = 6 mg/L, $C^{in}_{O,g}$ = 275 mg/L, $C^{in}_{S,\ell}$ = 20 mg/L, ρ_v = 75 000 mg/L).

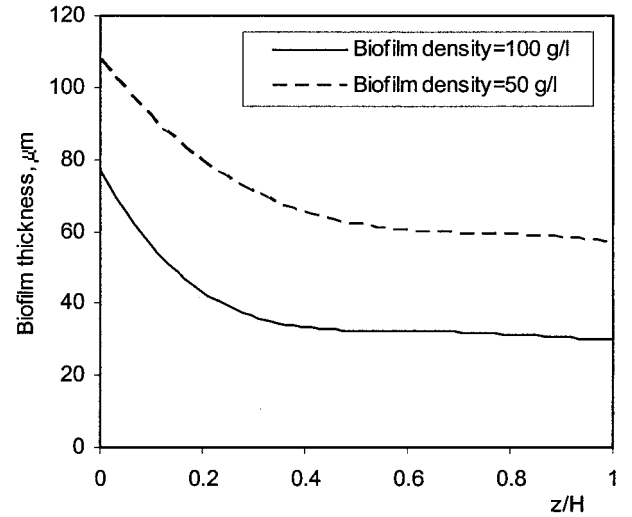

Figure 7. Longitudinal variations of biofilm thickness ($C^{in}_{O,\ell}$ = 6 mg/L, $C^{in}_{O,g}$ = 275 mg/L, $C^{in}_{S,\ell}$ = 30 mg/L, t = 3200 min).

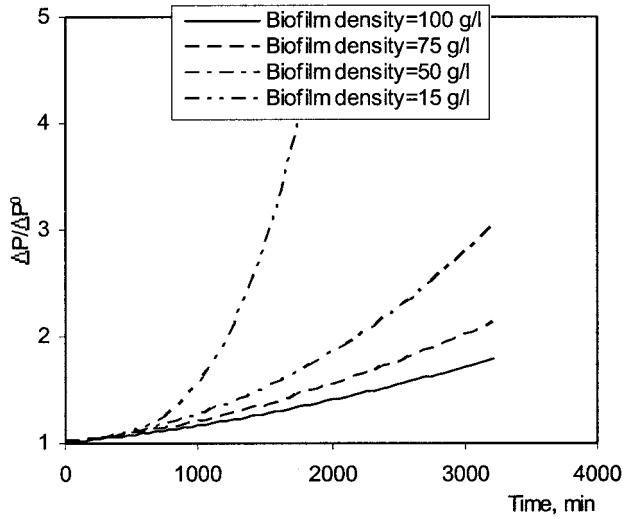

Figure 8. Two-phase pressure drop ratio vs. time at different values of total dry biomass in the biofilm ($C^{in}_{O,\ell}$ = 6 mg/L, $C^{in}_{O,g}$ = 275 mg/L, $C^{in}_{S,\ell}$ = 30 mg/L).

two-phase pressure drop ratio (Figure 8). Variation of biofilm thickness with biofilm dry density has been reported by several investigators (Hoehn and Ray, 1973; Shieh et al., 1981; Timmermans and van Haute, 1984; Tang et al., 1987, Tang and Fan, 1987). However, the increase of biofilm thickness, with the decrease of total dry biomass in the biofilm, does not mean a higher value of the biodegradation rate. Figure 9 shows the predicted outlet phenol concentration plotted as a function of inlet phenol concentration at different values of the total dry biomass in the biofilm. The outlet-phenol concentration is lower at higher value of total dry biomass in the biofilm, which means higher biodegradation rate in this case. Additionally, the outlet concentration is lower for lower values of the inlet

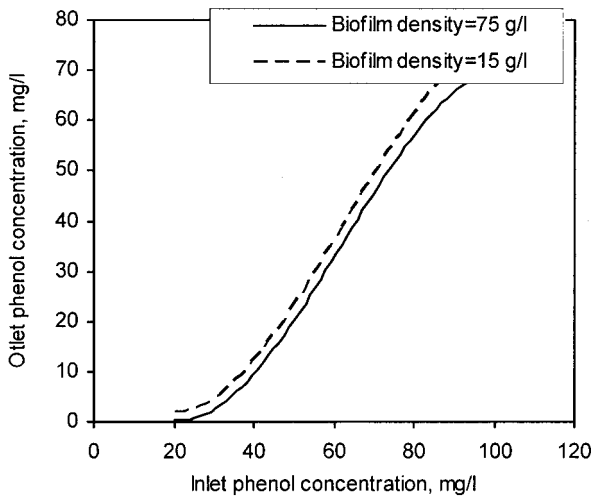

Figure 9. Outlet phenol concentration vs. inlet phenol concentration at different values of total dry biomass in the biofilm ($C^{in}_{O,\ell}$ = 6 mg/L, $C^{in}_{O,g}$ = 275 mg/L).

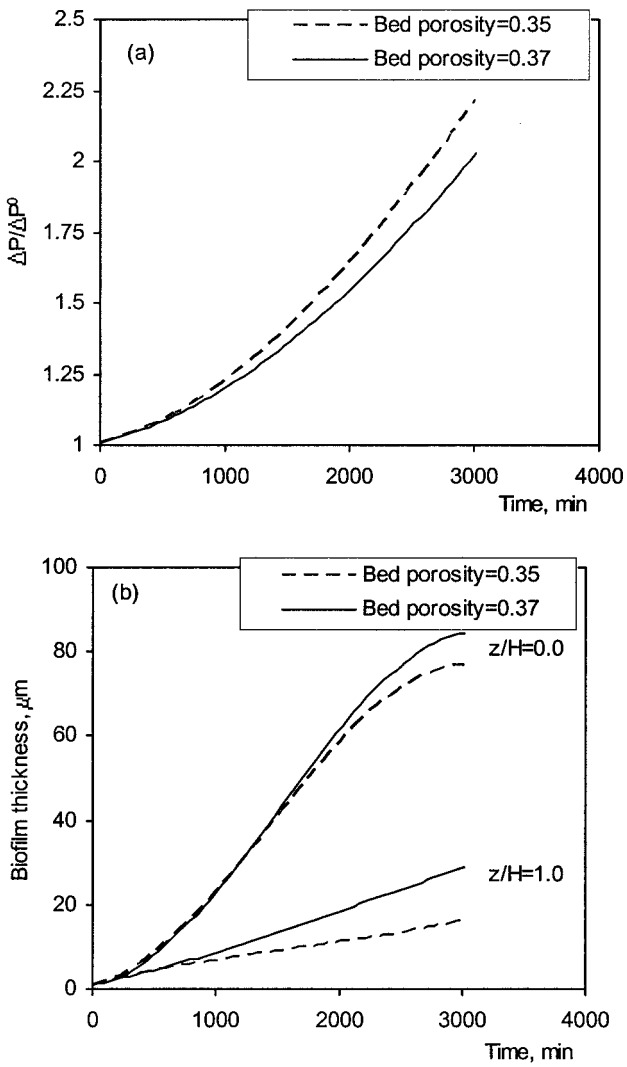

Figure 10. (a) Two-phase pressure drop buildup; (b) and biofilm thickness vs. time at different values of bed porosity ($C^{in}_{O,\ell}$ = 6 mg/l, $C^{in}_{O,g}$ = 275 mg/L, $C^{in}_{S,\ell}$ = 30 mg/L, ρ_v = 75 000 mg/L).

phenol concentration and rises sharply when the inlet-phenol concentration is increased beyond about 40 mg/L.

Figures 10a and 11a show the effect of bed porosity and particle diameter on the pressure drop buildup. Although, at lower-bed porosity or particle diameter, the biofilm thickness is lower (Figures 10b and 11b), the rise of the pressure drop is higher. Even if lower-bed porosity (or particle diameter) induces thinner biofilms, biomass volume ($a^o_s\delta_b$) is higher as a result of the higher specific area of the packing.

Conclusion

Excessive biomass formation in two-phase flow trickle-bed bioreactors develops clogging, and leads to the progressive obstruction of the bed, that is accompanied with a buildup in pressure drop and flow channeling. Clogging is a complex phenomenon determined by such diverse factors as the biological and physical characteristics of the compounds involved, and the structural characteristics of the packing material. A 1-D

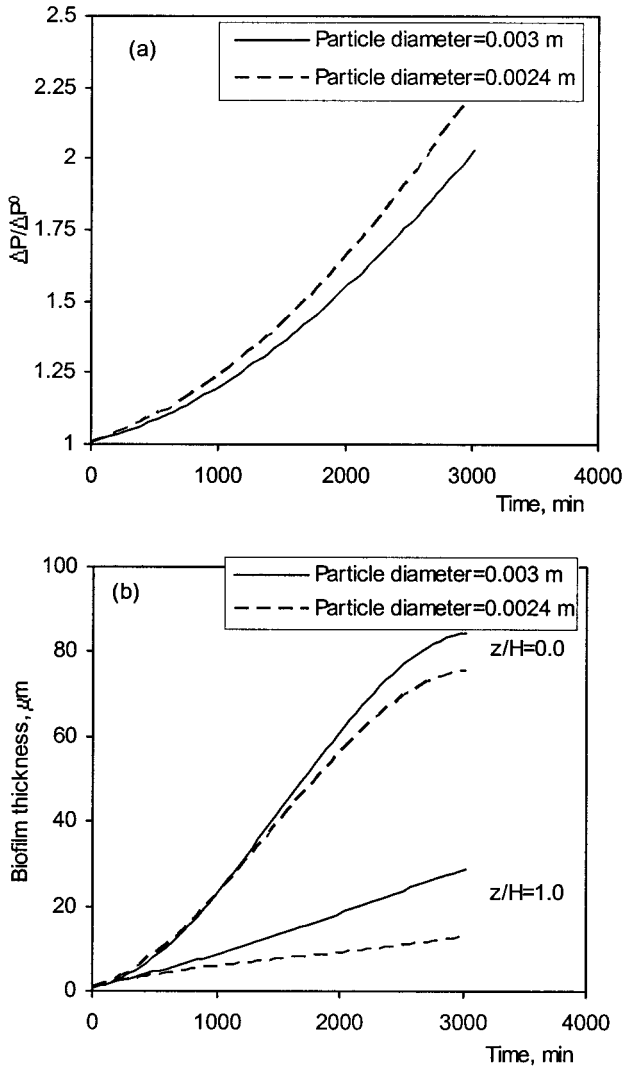

Figure 11. (a) Two-phase pressure drop ratio, and (b) biofilm thickness versus time at different values of particle diameter ($C^{in}_{O,\ell}$ = 6 mg/L, $C^{in}_{O,g}$ = 275 mg/L, $C^{in}_{S,\ell}$ = 30 mg/L, ρ_v = 75 000 mg/L).

transient two-fluid dynamic model, based on the macroscopic volume-averaged mass and momentum balance equations and volume-averaged species balance equations at the reactor level, coupled with the simultaneous transport and consumption of phenol and oxygen within the biofilm, and with the simultaneous diffusion of both phenol and oxygen and adsorption of phenol within the activated carbon particles, was proposed for the description of two-phase flow and space-time evolution of clogging in trickle flow bioreactors. The phenol biodegradation by *Pseudomonas putida* as the predominant species immobilized on activated carbon was chosen as a case study illustrating the consequences of formation of excessive amount of biomass.

Notation

a_s^o = specific area of the packing (surface of the particles/volume of the bed), m^2/m^3
a_{sb} = specific area of the bioparticle, $m^2/m^3_{bioparticle}$
C_j = concentration of component j (j = O_2, PhOH), kg/m^3
$C_{j,w}$ = concentration of component j in the biofilm when the external surface area of the biocatalyst particle is completely wetted (j = O_2, PhOH), kg/m^3
$C_{j,d}$ = concentration of component j in the biofilm when the external surface area of the biocatalyst particle is completely dry (j = O_2, PhOH), kg/m^3
D_j = molecular diffusivity of component j, m^2/s
D_j^{eff} = effective diffusivity of component j, m^2/s
D_ℓ = liquid axial dispersion coefficient, m^2/s
d_b = bioparticle diameter, m
d_p = particle diameter, m
E_1, E_2 = Ergun constants
$F_{g\ell}$ = gas-liquid drag force, N/m^3
F_{gs} = gas-solid drag force, N/m^3
$F_{\ell s}$ = liquid-solid drag force, N/m^3
g = gravitational acceleration, m/s^2
H = bed height, m
He = Henry constant
K_i = inhibition constant, kg/m^3
K_{ox} = saturation constant of oxygen, kg/m^3
K_S = saturation constant of phenol, kg/m^3
k_{gs} = gas-solid mass-transfer coefficient, m/s
$k_\ell a$ = volumetric liquid-side mass-transfer coefficient, s^{-1}
k_s = liquid-solid mass-transfer coefficient, m/s
P = pressure, Pa
q = amount of phenol adsorbed per unit weight of activated carbon
r = radial position within bioparticle, m
r_b = radius of the bioparticle, m
r_p = radius of the support particle (m)
r_X = cell growth rate, $r_X = \mu\rho_v$, kg/m^3s
t = time, s
u_α = average interstitial velocity of α-fluid, m/s
u^* = interfacial velocity, m/s
v_α = α-phase superficial velocity, m/s
$Y_{X/O}$ = yield coefficient, kg biomass/kg oxygen
$Y_{X/S}$ = yield coefficient, kg biomass/kg phenol
z = axial coordinate, m

Greek Letters

δ_b = biofilm thickness, m
ε = bed porosity
ε_b = porosity of biofilm
ε_g = gas holdup
ε_ℓ = liquid holdup
ε_p = particle porosity
η_g = effectiveness factor for a completely dry particle
η_e = external wetting efficiency
η_ℓ = effectiveness factor for a fully wetted particle
η_G = overall effectiveness factor,
μ = specific growth rate, s^{-1}
μ_{max} = maximum specific growth rate, s^{-1}
μ_α = α phase dynamic viscosity, kg/m · s
μ_α^e = α phase effective viscosity (combination of bulk and shear terms), kg/m · s
ρ_c = dry cell mass/wet cell volume, kg/m^3
ρ_v = total dry biomass in the biofilm, kg/m^3
ρ_α = density of α phase, kg/m^3

Subscripts/Superscripts

b = biofilm
g = gas
in = inlet
ℓ = liquid
O = oxygen
s = solid phase
S = phenol
o = clean bed state
$*$ = on byocatalyst surface

Literature Cited

Alonso, C., M. T. Suidan, G. A. Sorial, F. L. Smith, P. Biswas, P. J. Smith, and R. C. Brenner, "Gas Treatment in Trickle-Bed Biofilters: Biomass, How Much is Enough?," *Biotechnol. and Bioeng*., **54**, 583 (1997).

Arters, D. C., and L. -S. Fan, "Solid-Liquid Mass Transfer in a Gas-Liquid-Solid Fluidized Bed," *Chem. Eng. Sci.*, **41**, 107 (1986).

Chen, X., and P. S. Stewart, "Biofilm Removal Caused by Chemical Treatments," *Water Res*., **34**, 4229 (2000).

Chiam, H. F., and I. J. Harris, "Application of a Noninhibitory Growth Model to Predict the Transient Response in a Chemostat," *Biotechnol. and Bioeng*., **25**, 1613 (1983).

Cox, H. H. J., and M. A. Deshusses, "The Use of Protozoa to Control Biomass Growth in Biological Trickling Filters for Waste Air Treatment," Proc. of the 90th Annual Meeting and Exhibition on the Air and Waste Management Association, Toronto, Ont., Air and Waste Management Association, Pittsburgh, PA (June 8-13, 1997).

Cox, H. H. J., and M. A. Deshusses, "Biomass Control in Waste Air Biotrickling Filters by Protozoan Predation," *Biotechnol. and Bioeng*., **62**, 216 (1999).

Dankworth, D.C., I.G. Kevrekidis, and S. Sundaresan, "Dynamics of Pulsing in Trickle Beds," *AIChE J.*, **36**, 605 (1990).

Delhoménie, M.-C., L. Bibeau, J. Gendron, R. Brzezinski, and M. Heitz, "A Study of Clogging in a Biofilter Treating Toluene Vapors," *Chem. Eng. J*., **94**, 211 (2003).

Deshusses, M. A., G. Hamer, and I. J. Dunn, "Behavior of Biofilters for Waste Air Biotreatment. 1. Dynamic model development," *Environ. Sci. Technol*., **29**, 1048 (1995).

Diks, R. M. M., S. P. P. Ottengraff, and A. H. C. van den Oeven, "The Influence of NaCl on the Degradation rate of Dichloromethane by *Hyphomicrobium* sp," *Biodegradation*, **5**, 129 (1994).

Goto, S., and J. M. Smith, "Trickle-Bed Reactors Performance, Part -1: Holdup and Mass Transfer Effects," *AIChE J.*, **21**, 706(1975).

Gresho, P. M., and R. L. Sani, *Incompressible Flow and the Finite Element Method. Advection-Diffusion and Isothermal Laminar Flow*, Wiley, Chichester, U.K. (1988).

Hirata, A., Y. Hosaka, and H. Umezawa, "Biological Treatment of Water and Wastewater in Three-Phase Fluidized Bed," *Proc. 3rd World Cong. Chem. Eng.*, III, 556, Tokyo (1986).

Hoehn, R. G., and A. D. Ray, "Effects of Thickness on Bacterial Film," *J. Water Poll. Control Fed.*, **45**, 2302 (1973)

Holub, R.A., M.P. Dudukovic, and P.A. Ramachandran, "A phenomenological Model of Pressure Drop, Liquid Holdup and Flow Regime Transition in Gas-Liquid Trickle Flow," *Chem. Eng. Sci.*, **47**, 2343 (1992).

Iliuta, I., "Performance of Fixed Bed Reactors with Two-Phase Upflow and Downflow," *J. Chem. Tech. Biotechnol.,* **68***,* 47 (1997).

Iliuta, I., F. Larachi, and B. P. A. Grandjean, "Pressure Drop and Liquid Hold-Up in Trickle Flow Reactors: Improved Ergun Constants and Slip Correlations for the Slit Model," *Ind. Eng. Chem. Res.*, **37**, 4542 (1998).

Iliuta, I., A. Ortiz, F. Larachi, B. P. A. Grandjean, and G. Wild, "Hydrodynamics & Mass Transfer in Trickle-Bed Reactors: An Overview," *Chem. Eng. Sci*., **54**, 5329 (1999).

Iliuta, I., F. Larachi, and M. H. Al-Dahhan, "Double-Slit Model for Partially Wetted Trickle Flow Hydrodynamics," *AIChE J.*, **46**, 597 (2000).

Iliuta, I., B. P. A. Grandjean, and F. Larachi, "New Mechanistic Film Model for Pressure Drop and Liquid Holdup in Trickle Flow Reactors," *Chem. Eng. Sci.*, **57**, 3359 (2002).

Iliuta, I., F. Larachi, and B. P. A. Grandjean, "Fines Deposition Dynamics in Trickle Flow Reactors," *AIChE J.*, **49**, 485 (2003).

Iliuta, I., and F. Larachi, "Fines Deposition Dynamics in Packed-Bed Bubble Reactors," *Ind. Eng. Chem. Res.*, **42**, 2441 (2003).

Kato, Y., A. Nishiwaki, T. Fukuda, and S. Tanaka, "The Behavior of Suspended Solid Particles and Liquid in Cubble Columns," *J. Chem. Eng. Japan*, **5**, 112 (1972).

Larachi, F., L. Belfares, and B. P. A. Grandjean, "Prediction of Liquid-Solid Wetting Efficiency in Trickle Flow Reactors," *Int. Commun. of Heat and Mass Transfer*, **28**, 595 (2001a).

Larachi, F., L. Belfares, I. Iliuta, and B. P. A. Grandjean, "Three-Phase Fluidization Macroscopic Hydrodynamics - Revisited Macroscopic Hydrodynamics of Three-Phase Fluidization - Tentative Exegesis," *Ind. Eng. Chem. Res*., **40**, 993 (2001b).

Larachi, F., L. Belfares, I. Iliuta, and B. P. A. Grandjean, "Heat and Mass Transfer in Co-Current Gas-Liquid Packed Beds Analysis, Recommendations and New Correlations," *Ind. Eng. Chem. Res*., **42**, 222 (2003).

Laurenzis, A., H. Heits, S. -M. Wubker, U. Heinze, C. Friedrich, and U. Werner, "Continuous Biological Waste Gas Treatment in a Stirred Trickle-Bed Reactor with Discontinuous Removal of Biomass," *Biotechnol. Bioeng.*, **57**, 497 (1998).

Leson, G. and A. M. Winer, "Biofiltration: An Innovative Air Pollution Control Technology for VOC Emissions," *J. Air Waste Manag. Assoc*., **41**, 1045 (1991).

van Lith, C. P. M., S. P.P. Ottengraf, and R. M. M. Diks, " The Control of a Biotrickling Filter," *VDI Berichte*, **1104**, 169 (1994).

Liu, S., A. Afacan, and J. Masliyah, "Steady Incompressible Laminar Flow in Porous Media," *Chem. Eng. Sci*., **21**, 3565 (1994).

Okkerse, W. J. H., S. P.P. Ottengraf, B. Osinga-Kuipers, and M. Okkerse, "Biomass Accumulation and Clogging in Biotrickling Filters for Waste Gas Treatment. Evaluation of the Dynamic Model Using Dichloromethane as a Model Pollutant," *Biotechnol. and Bioeng*., **63**, 418 (1999).

Ottengraff, S. P. P., A. H. C. van der Oever, and F. J. C. M. Kempenaars, " Waste Gas Purification in a Biological Filter Bed," *Prog. Ind. Microbiol*., **20**, 157 (1984).

Ottengraff, S. P. P., J. J. P. Meesters, A. H. C. Van den Oever, and H. R. Rozema, "Biological Elimination of Volatile Xenobiotic Compounds in Biofilters," *Bioprocess Eng.*, **1**, 61.

Piché, S., F. Larachi, I. Iliuta, and B. P. A. Grandjean, "Improving Predictions of Liquid Back-Mixing in Trickle-Bed Reactors Using a Neural Network Approach," *J. Chem. Technol. & Biotechnol*., **77**, 989 (2002).

Ramachandran, P. A., and J. M. Smith, "Effectiveness Factors in Trickle-Bed Reactors," *AIChE J*., **25**, 538 (1979).

Schonduve, P., M. Sara, and A. Friedl, "Influence of Physiologically Relevant Parameters on Biomass Formation in a Trickle-Bed Bioreactor Used for Waste Gas Cleaning," *Appl. Microbiol. Biotechnol.*, **45**, 286 (1996).

Schroeder, E. D., "Trends in Application of Gas-Phase Bioreactors," *Rev. in Env. Sci. & Bio/Technol*., **1**, 65 (2002).

Shah, Y. T., B. G. Kelkar, S. P. Godbole, and W. D. Deckwer, "Design Parameters Estimation for Bubble Column Reactors," *AIChE J.*, **28**, 353 (1982).

Shieh, W. K., P. M. Sutton, and P. Kos, "Predicting reactor Biomass Concentration in a Fluidized-Bed System," *J. Water Poll. Control Fed.*, **53**, 1574 (1981).

Sorial, G. A., F. L. Smith, M. T. Suidan, and P. Biswas, "Evaluation of a Trickle Bed Biofilter Media for Toluene Removal," *J. Air Waste Manag. Assoc.*, **45**, 801 (1995).

Tang, W. -T., and L. -S. Fan, "Steady State Phenol Degradation in a Draft-Tube, Gas-Liquid-Solid Fluidized-Bed Bioreactor," *AIChE J.,* **33,** 239 (1987).

Tang, W. -T., K. Wisecarver, and L. -S. Fan, "Dynamics of a Draft Tube Gas-Liquid-Solid Fluidized Bed Bioreactor for Phenol Degradation," *Chem. Eng. Sci.,* **42**, 2123 (1987).

Timmermans, P., and A. van Haute, "Influence of the Type of Organisms on the Biomass Hold-Up in Fluidized-Bed Reactor," *Appl. Microbiol. Biotechnol.*, **19**, 36 (1984).

Weber, F. J., and S. Hartmans, "Toluene Degradation in a Trickle-Bed Reactor - Prevention of Clogging," *VDI Berichte*, **1104**, 161 (1994).

Weber, F. J., and S. Hartmans, "Prevention of Clogging in a Biological Trickle-Bed Reactor Removing Toluene From Contaminated Air," *Biotechnol. and Bioeng*., **50**, 91 (1996).

Wisecarver, K. D., and L. -S. Fan, "Biological Phenol Degradation in a Gas-Liquid-Solid Fluidized Bed Reactor," *Biotechnol. and Bioeng*., **33**, 1029 (1989).

Whitaker, S., "The Transport Equations For Multi-Phase Systems," *Chem. Eng. Sci*., **28**, 139 (1973).

Wübker, S.M., A. Laurenzis, U. Werner, and C. Friedrich, "Controlled Biomass Formation and Kinetics of Toluene Degradation in a Bioscrubber and in a Reactor with Periodically Moved Trickle-Bed," *Biotechnol. and Bioeng*., **55**, 686 (1997).

Manuscript received Aug. 19, 2003, and revision received Jan. 21, 2004.